Editors' Suggestion

Ultralow effective interfacial tension between miscible molecular fluids

Alessandro Carbonaro,* Luca Cipelletti, and Domenico Truzzolillo
Laboratoire Charles Coulomb (L2C), UMR 5221 CNRS-Université de Montpellier, Montpellier, France

(Received 21 March 2020; accepted 4 June 2020; published 10 July 2020)

We exploit the deformation of drops spinning in a denser background fluid to investigate the effective interfacial tension (EIT) between miscible molecular fluids. We find that, for sufficiently low interfacial tension, spinning drops develop dumbbell shapes, with two large heads connected by a thinner central body. We show that this shape depends not only on the density and viscosity contrast between the drop and background fluids, but also on the fluid molecular structure, and hence on the stresses developing at their interface due to a different molecular interaction. We systematically investigate the dynamics of dumbbell-shaped drops of water-glycerol mixtures spinning in a pure glycerol reservoir. By developing a model for the deformation based on the balance of the shear stress opposing the deformation, the imposed normal stress on the drop, and an effective interfacial tension, we exploit the time evolution of the drop shape to measure the EIT. Our results show that the EIT in water-glycerol systems is orders of magnitude lower than that reported in previous experimental measurements, and in excellent agreement with values calculated via the phase field model proposed by Truzzolillo *et al.* [Phys. Rev. X **6**, 041057 (2016)].

DOI: 10.1103/PhysRevFluids.5.074001

I. INTRODUCTION

Interfacial tension between immiscible fluids is a well-defined, well-known quantity of paramount importance in a wide range of phenomena, from soft matter and material science to biophysics, oil recovery and multiphase flow [1]. By contrast, the presence of capillary stresses at the interface between miscible fluids is still debated and actively investigated. For miscible fluids, equilibrium thermodynamics states that interfacial tension should not exist, the equilibrium state being a homogeneous mixture of the fluids. However, transient capillary stresses between miscible fluids were first postulated in 1901 by Korteweg, who asserted that stresses due to density (or composition) gradients in a multifluid system could act as an effective interfacial tension (EIT) [2]. Following his work, one can write the EIT, hereinafter denoted by Γ_e, similarly to the tension at equilibrium between immiscible fluids, i.e., by expanding the mixing free energy in even powers of the concentration gradient $\nabla\tilde{\varphi}$ [3]. By considering only the first term of this expansion, Γ_e can be written as

$$\Gamma_e = \int_{-\infty}^{+\infty} \kappa(\tilde{\varphi})(\nabla\tilde{\varphi})^2 dz. \tag{1}$$

Here $\tilde{\varphi}$ is the space-dependent volume fraction of one of the two fluids, z is the coordinate orthogonal to the interface, and $\kappa(\tilde{\varphi})$ is the so-called Korteweg parameter, embedding the effect of the specific interaction between the fluids [4,5]. Clearly, Γ_e tends to zero with time t, as diffusion smears out the interface, whose thickness increases, reducing $\nabla\tilde{\varphi}$ with t [6]. Such a transient, out-of-equilibrium interfacial tension has been invoked in literature to rationalize the behavior of miscible fluids at short

*alessandro.carbonaro@umontpellier.fr

times, before they are fully mixed, and several works tried to elucidate the role of stresses at miscible boundaries, both theoretically [7–12] and experimentally. Among the strategies adopted to measure the EIT between miscible fluids, the most recent ones leverage on the study of hydrodynamic instabilities [5,13], on light scattering experiments probing capillary waves [6,14], and on the observation of the shape of drops and threads under an external forcing [15–17]. Despite this effort, the magnitude and even the very existence of EIT between simple molecular fluids is still debated and mostly unclear.

One technique to measure very low interfacial tensions (10^{-3}–10^{-2} mN/m [18,19]) is spinning drop tensiometry (SDT), which is based on the observation of drop shapes. In an SDT experiment a drop is injected in a denser background fluid contained in a cylindrical capillary. When the capillary is spun, the drop elongates on the axis of rotation due to centrifugal forces. Following the drop shape by means of video imaging, one can then measure the interfacial tension between the drop and the background fluid. In the case of immiscible fluids, for which SDT was initially conceived by Vonnegut [20], one typically measures the equilibrium shape of the drop, which is dictated by the balance between surface tension and centripetal forces. The interfacial tension Γ is then obtained through the Vonnegut equation [20]:

$$\Gamma = \frac{\Delta\rho\omega^2 r^3}{4}, \tag{2}$$

where $\Delta\rho$ is the density difference between the background and drop fluids, ω the angular velocity, and r the equilibrium radius of the drop. A second possibility is to characterize the time evolution of the drop after a sudden rotational speed jump. Recently, we have employed this technique to study the elongation dynamics of drops, both in miscible and immiscible background fluids [16], showing that the drop dynamics towards an equilibrium state are characterized by a relaxation time fully determined by (i) the viscosity of the fluids, (ii) the drop size, and (iii) the interfacial tension. In the past few decades, SDT experiments aiming at characterizing equilibrium states and diffusion processes have been performed by several groups to investigate the presence and the relevance of an EIT between miscible fluids, either close to [15,21] or far from a spinodal decomposition of the fluids [22,23]. Unfortunately, in the case of fully miscible molecular liquids, such as water and glycerol, diffusion hampers the measurement of stationary states and literature data are conflicting, sometimes even in experiments by the same authors [23,24]. Indeed, when Γ is negligible a stationary state is never attained, as we showed for one specific pair of miscible fluids with small compositional mismatch, namely a drop of a water-glycerol mixture (5 wt % H_2O) spinning in pure glycerol. As a result, the question of whether an EIT exists or not in such a case has not been settled yet.

SDT experiments at low Γ are furthermore complicated by the fact that drops do not always maintain a simple ellipsoidal shape. Even for immiscible fluids, for sufficiently low interfacial tensions, they can develop a "dumbbell" or "dog-bone" shape consisting of two large heads connected by a thinner central body, as reported in the case of water-hydrocarbon-surfactant systems with $\Gamma < 10\ \mu$N/m [25]. In this case a satisfactory explanation of the phenomenon is still lacking. More recently [22], such shapes have been also observed in miscible fluids and have been attributed to the effect of perturbation due to viscous secondary flows in finite reservoirs of rotating fluids. Such an effect, till now unexplored, is the focus of the present work.

To set the scene, Fig. 1 shows examples of such dumbbell shapes for drops rotating in a pure glycerol reservoir. Drops in panels A and C are composed of mixtures of water and glycerol, respectively with water mass concentration $c_w = 0.75$ and $c_w = 0.20$, whereas the drop in panel B is made of triethylene glycol (TEG). All drops are fully miscible with the glycerol background. Strikingly, Fig. 1 shows that the development of a dumbbell shape depends not only on the density and viscosity contrast with respect to the background fluid, but also on the molecular structure of the fluids. Indeed, in absence of any interfacial stresses, the TEG drop should have an intermediate shape between drops in panels A and C, since it has intermediate density and viscosity. This is evidently not the case; consequently, Fig. 1 cannot be explained only by means of hydrodynamic

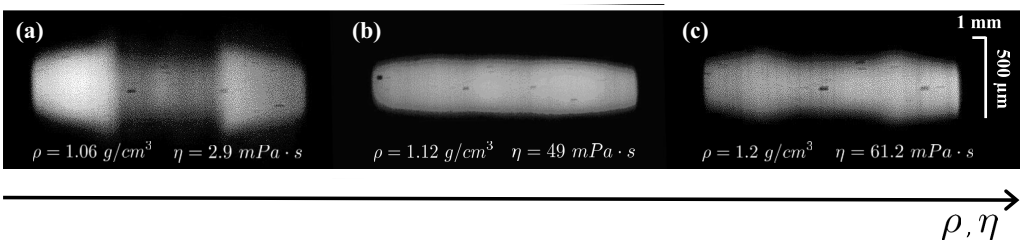

FIG. 1. Dyed drops containing 75% H_2O–25% glycerol (panel A), TEG (panel B), and 20% H_2O–80% glycerol (panel C). All drops spin in a reservoir of pure glycerol. Images are optically compressed in the horizontal direction and expanded in the vertical direction to improve resolution, as detailed in the main text (Sec. II).

arguments. Thus, characterizing the evolution of such drop shapes appears to be a promising strategy to measure the effect of interfacial stresses between the drop and background fluids. In this work, we tackle this challenging task and investigate experimentally the time evolution and the origin of dumbbell-shaped drops by systematically varying the composition of the drop fluid in a series of SDT experiments. Furthermore, we exploit fluorescent drops to track the time evolution of the full concentration profile of the fluids in the capillary, instead of simply measuring the intensity profile of the collected light. We model the temporal dynamics of the drop shape by balancing the normal stress imposed on the drop surface, the shear stress opposing the deformation, and the effect of an EIT, and we exploit the deformation dynamics to measure the effective interfacial tension between miscible molecular fluids.

The rest of the work is organized as follows. In Sec. II we present the setup and materials employed, and elucidate the procedure to extract the concentration profile of the fluids in the capillary. In Sec. III we present the data on the deformation dynamics of drops, discussing our results in the light of a model allowing one to measure Γ_e. Finally, in Sec. IV we make some concluding remarks and summarize the key results of our work.

II. MATERIALS AND METHODS

Glycerol ($\geqslant$99.5 wt %) was purchased from Sigma Aldrich and used as received. Water-glycerol mixtures were prepared using Milli-Q ultrapure water, with densities ρ and viscosities η reported in Table I as a function of water mass fraction c_w, for $T = 25.0 \pm 0.5\,^{\circ}$C. The water mass fraction was determined via rheological measurements as detailed in Table I. Fluorescein (disodium salt) was purchased from Merck KGaA and dissolved in the drop fluids at two concentrations, 2×10^{-3} wt/wt and 10^{-3} wt/wt, for two independent sets of measurements as detailed later. Experiments were performed with a Krüss spinning drop tensiometer at $25.0 \pm 0.5\,^{\circ}$C, with rates of rotation ranging from 6000 to 15 000 rpm, so that buoyancy could be neglected. All drops were injected with a 1 μl syringe in a capillary with an internal diameter of 3.25 mm, prefilled with glycerol before each experiment. The time between the injection and the beginning of the rotation was typically 10–15 seconds. After each measurement, the fluids were replaced and a fresh new drop was injected in the capillary. To image the drops, the tensiometer is equipped with a blue LED with dominant wavelength of 469 nm for illumination and a CMOS camera (Toshiba Teli BU406M) for imaging. Since the drops become very elongated, we use as an objective two cylindrical lenses (Newport CKX17-C) that expand the field of view in the horizontal direction x and compress it in the vertical direction y. As described in [16], the resulting magnification in the x (horizontal) direction is $M_x = 0.3$, while the magnification in the y (vertical) direction is $M_y = 3.36$. The different horizontal and vertical magnifications allow one to follow the dynamics of very elongated drops along almost all the capillary length (5 cm), while gaining at the same time in accuracy along the vertical direction.

TABLE I. Densities and viscosities of the water-glycerol mixtures used in the experiments.

Liquid	ρ (g/cm^3)[a]	η (mPa s)[b]
Glycerol[c] ($c_w \leqslant 0.02$)	1.26 ± 0.01	800.0 ± 0.1
$c_w = 0.25$	1.19 ± 0.01	33.8 ± 0.1
$c_w = 0.45$	1.12 ± 0.01	9.0 ± 0.1
$c_w = 0.70$	1.07 ± 0.01	2.8 ± 0.1
$c_w = 0.75$	1.06 ± 0.01	2.3 ± 0.1
$c_w = 0.90$	1.02 ± 0.01	2.2 ± 0.2
Water[d]	0.996 ± 0.001	0.89 ± 0.01

[a]Densities of water-glycerol mixtures were obtained from tabulated values [26] corresponding to mixtures having the measured zero-shear viscosities.
[b]The viscosities of water-glycerol mixtures and pure glycerol were measured by performing steady rate rheology experiments using a stress-controlled AR 2000 rheometer (TA Instruments) with a steel cone-and-plate geometry (cone diameter = 50 mm, cone angle = 0.0198 rad). No dependence of the viscosity on the shear rate was observed as all samples showed pure Newtonian response.
[c]The viscosity of the glycerol used as the background fluid is lower than that tabulated for anhydrous glycerol [26] because of the unavoidable adsorption of water from the atmosphere.
[d]The viscosity and the density of water were measured using a rolling-ball Anton Paar Lovis 2000ME microviscosimeter and a DMA 4500M densimeter, respectively.

Following the magnification stage, a blue light filter in front of the CMOS eliminates the blue background light.

A. Concentration profiles

An example of the optically compressed images of the drops obtained with the experimental setup is shown in Fig. 2(a), displaying the typical time evolution of a drop of pure water spinning in pure glycerol. A further step is required to follow more precisely the evolution of the interface. To this end, we extract the concentration profile of the drop fluid from the fluorescence intensity, in order to define precisely the drop boundary. Note that, strictly speaking, the fluorescence signal

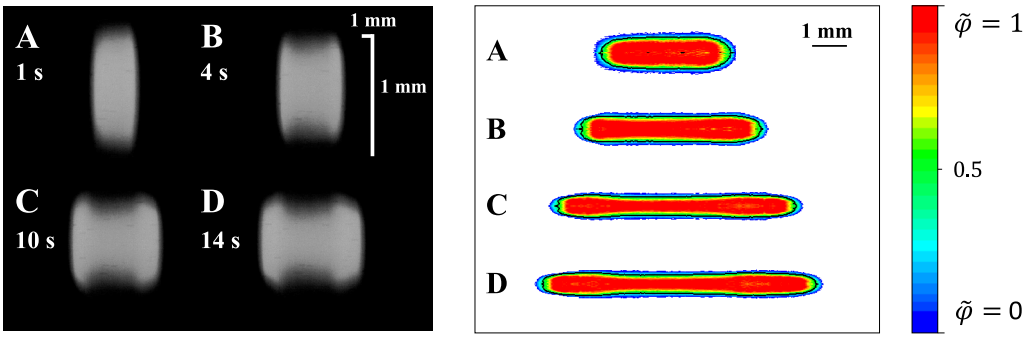

FIG. 2. (a) Time evolution of the fluorescence intensity recorded for a typical drop of pure water in a pure glycerol background. Note the different magnification in the horizontal and vertical directions. (b) Concentration profiles reconstructed from the fluorescence intensity images of panel (a), as detailed in the text. In panel (b), the scale is the same in the horizontal and vertical directions. The black line represents the drop surface, defined as the set of points where $\tilde{\varphi}(x, r) = 0.5$.

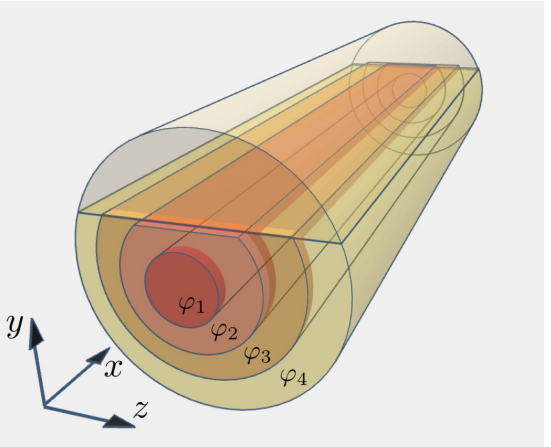

FIG. 3. Scheme of the drop for the inversion routine to retrieve the concentration profile from the fluorescence intensity. We typically use $N = 204$ shells; for clarity, only the first four shells are shown here. The fluorescence intensity distribution generally varies along the x direction, yielding an x-dependent concentration profile for the drop fluid $\tilde{\varphi}(x, r)$.

comes from the spatial distribution of fluorescein, not that of the drop fluid. However, over the timescale of our experiments (∼10 s) we assume the concentration profile of fluorescein to closely follow the one of the drop fluid, since there is not enough time to develop an appreciable difference in distribution of the two components. To support this claim, we compare the diffusion coefficients of water (the drop fluid) and of fluorescein in the background glycerol. The self diffusion coefficient of water is $D_w = 1.025 \times 10^{-9}$ m^2/s and the diffusion coefficient of water in glycerol is $D_{wg} = 1.4 \times 10^{-11}$ m^2/s [27]. On the other hand, the diffusion coefficient of fluorescein in water is $D_{fw} = 6.4 \times 10^{-10}$ m^2/s [28]. We estimate the diffusion coefficient of fluorescein in glycerol as $D_{fg} \simeq D_{fw}\frac{D_{wg}}{D_w} \simeq 8.7 \times 10^{-12}$ m^2/s. Therefore, the difference between the distances over which water and fluorescein may diffuse over the time scale of our experiments is $l_w - l_f \approx 3$ μm, much smaller than the resolution with which we measure the drop shape, which we determine to be a few tens of μm. Consequently, we can safely assume the concentration profile of the fluorophore to represent well that of the drop fluid. Furthermore, by changing the concentration of fluorophore over more than one decade (from 1×10^{-4} wt/wt to 2.5×10^{-3} wt/wt), we tested that the concentration of fluorescein is directly proportional to the light intensity collected.

These considerations, together with an additional symmetry argument, allow linking the intensity of the collected light to the x dependent radial concentration profile of the drop fluid. Exploiting the cylindrical symmetry of the drops, one can move from a bidimensional intensity image to a three-dimensional concentration map.

In order to do so, we divide the drop into N concentric cylindrical shells of radius r_i and constant thickness dr, each of them having a local value of water volume fraction $\tilde{\varphi}_i$ (see Fig. 3). The fluorescence intensity at a given horizontal coordinate x and vertical coordinate y is be given by the sum over the contributions of each shell, weighted by a geometric factor c_i proportional to the length of the chord that traverses such shell at coordinate y, along the z direction, i.e., the line of sight.

Accordingly, the intensity distribution reads

$$I(x_k, y_j) = \sum_{i=1}^{N} c_i(y_j)\tilde{\varphi}_i(x_k), \tag{3}$$

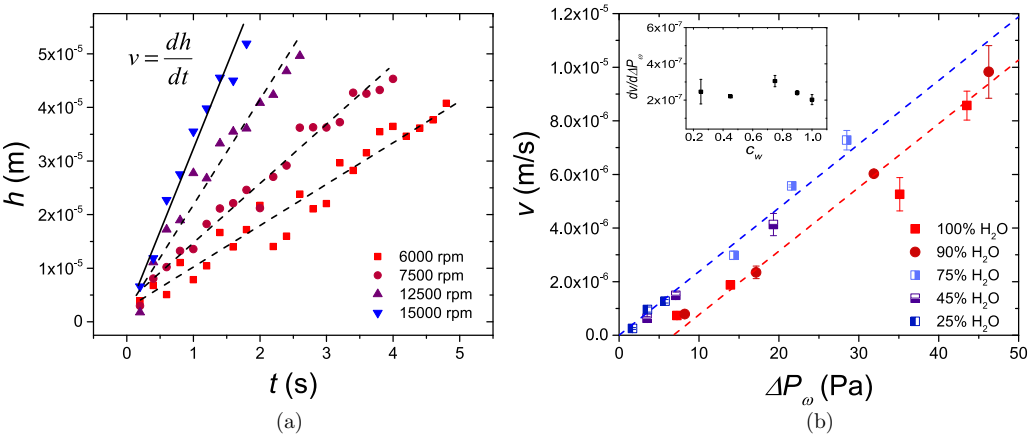

FIG. 4. (a) Time evolution of the deformation amplitude h for a drop of pure water in a pure glycerol background, at different ω as shown by the labels. (b) Deformation velocity as a function of the centripetal forcing, for various water mass fractions in the drop. The inset shows the slope of the velocity versus ΔP_ω, obtained by fitting independently datasets at a given c_w with a straight line.

where the indexes k and j have been introduced to account for the discretization of I on the pixel grid of the CMOS camera. For a given x_k, one can recast the problem in the matrix form

$$\mathbf{I} = \mathbf{C}\tilde{\varphi}, \tag{4}$$

with $\mathbf{I} = \{I_j\}$, $\mathbf{C} = \{c_{ji}\}$, and $\tilde{\varphi} = \{\tilde{\varphi}_i\}$; and $I_j \equiv I(x_k, y_j)$, $c_{ji} \equiv c_i(y_j)$, and $\tilde{\varphi}_i \equiv \tilde{\varphi}_i(x_k)$. For each k, the solution is thus $\tilde{\varphi} = \mathbf{C}^{-1}\mathbf{I}$. This procedure is mathematically equivalent to calculating a discrete version of the inverse Abel transform of the intensity distribution of the fluorescent light. Furthermore, the inversion of the matrix $\mathbf{C}$ is sped up by exploiting the symmetry of the drop around the longitudinal axis, which translates into the condition that $\mathbf{C}$ is lower-diagonal. By solving Eq. (4) for all x_k of interest, one obtains the concentration map of the the drop fluid in the capillary, as shown in Fig. 2(b). We use the maps to define the drop surface as the set of points where $\tilde{\varphi}(x, r) = 0.5$, with $\tilde{\varphi}(x, r)$ normalized to unity in the region of the drop close to the axis of rotation. The amplitude h of the drop deformation is defined as the difference between the maximum radius of the drop, close to the tips, and the minimum radius, at the center of the drop (see Fig. 5 below).

III. RESULTS AND DISCUSSION

We characterize the evolution of the drops towards a dumbbell shape by observing the time evolution of the deformation amplitude h, varying systematically the drop composition. Figure 4(a) shows the time evolution of h for a drop of pure water in pure glycerol, for various rotational speeds. Time $t = 0$ corresponds to the onset of the deformation, shortly after the start of rotation. At short time the deformation amplitude increases linearly with time, with a velocity $v = \frac{dh}{dt}$ that depends on the rotation speed. This dependence on ω stems from the fact that spinning drops are subject at the head of the drop to a rotation-induced pressure jump $\Delta P_\omega = \frac{1}{2}\Delta\rho\omega^2 r^2$ [16,29], where $\Delta\rho$ is the density difference between the denser background fluid and the drop and r the drop radius. This pressure jump ΔP_ω induces the drop elongation in first place, but it is also responsible for a secondary flow of the background fluid that leads to the dumbbell shape, as we shall detail below. Figure 4(b) reports the radial deformation velocity as a function of ΔP_ω, for various concentrations of water in the drops.

It is worth underlining two features. First, the velocity of the radial deformation is approximately a linear function of ΔP_ω, with a slope that is essentially independent of the concentration of water in the drop, as shown in the inset of Fig. 4(b). Second, even before trying to rationalize the dependence

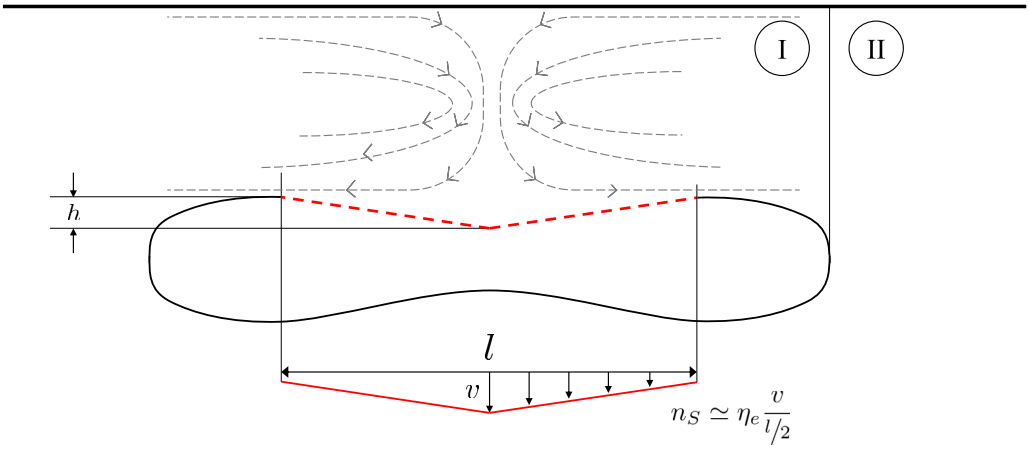

FIG. 5. Scheme of the drop deformation. The dashed arrows show the secondary flow of the background fluid induced by the capillary rotation.

of v on ΔP_ω, it appears clearly that the data may be divided in two main families. All data for drops with a mass concentration of water $c_w \leqslant 0.75$ are compatible with a straight line through the origin. By contrast, data from drops with $c_w = 0.9$ and $c_w = 1$ show a different behavior in that a linear fit of $v(\Delta P_\omega)$ displays a negative intercept with the v axis. This is counterintuitive if we were to neglect interfacial tension: drops containing a larger fraction of water, being less viscous, should be deformed more rapidly for a given centripetal forcing. Thus, the negative intercept of data for $c_w \geqslant 0.9$ strongly suggests a nonvanishing EIT for these systems. As a first step towards the modeling of our experiments, we perform a linear fit of two families of data in Fig. 4(b), for water concentrations up to $c_w = 0.75$ and above $c_w = 0.9$, respectively:

$$v = A\Delta P_\omega + B, \tag{5}$$

finding an R^2 value of 0.98 and 0.97 respectively, keeping the slope A the same for the two data families. The physical meaning of the terms A and B will be detailed later; however, we anticipate that B depends on the concentration c_w of water in the drop and hence on the EIT. It is thus crucial to perform a statistical analysis of the data of Fig. 4(b) in order to assess whether the difference in the offset B between data below and above $c_w = 0.9$ (semifilled and solid symbols, respectively) is statistically significant, or just due to experimental noise.

We perform a t test [30,31] on the difference between term B of the fit for the two data families, for $c_w \leqslant 0.75$ and $c_w \geqslant 0.9$. As detailed in [32], for the data of Fig. 4(b) the Student t distribution yields a value of the standardized variable $t = 6.43$. This is much larger than $t_{0.995} = 2.95$, the edge of the 1% confidence interval for a two-tailed t distribution with $N_1 + N_2 - 2 = 15$ degrees of freedom, where $N_1 = 9$ and $N_2 = 8$ are the numbers of data points in the two datasets. Hence we conclude that the difference between the B parameter for the two datasets in Fig. 4(b) is statistically significant, with a confidence level greater than 99%.

A. Model of the radial deformation and EIT

Having checked that the effect of the EIT on the data of Fig. 4(b) is statistically significant, we propose a simple model to rationalize the data and extract from them Γ_e. The model is based on the balance of all sources of stress on the drop interface at the onset of the deformation. Similarly to the approach by Lister and Stone in [29], we write an equilibrium equation for the stresses on the drop surface, at the center of the drop:

$$n_E = n_S + n_L, \tag{6}$$

where n_E is the normal stress inducing the deformation and n_S and n_L are the normal stresses opposing the deformation, with n_S the shear stress arising from the motion of the drop and background fluids and n_L a Laplace-like term that takes into account the effect of the EIT. Since in our experiments the viscosity η_e of the external background fluid is much higher than the viscosity η_d of the drop fluid, the shear stress can be approximated as $n_S \simeq 2\eta_e v/l$, where l is the distance over which the radial deformation develops as shown in Fig. 5. The Laplace-like term n_L is estimated as the difference between the Laplace pressure jump at the heads of the drop and that at the central body. At the onset of the deformation, the drop shape is well described by a cylinder with radius r_0 capped by two hemispheres. Consequently, the hemispherical heads and the cylindrical body will be characterized by a pressure jump with respect to the background fluid of $2\Gamma_e/r_0$ and Γ_e/r_0 respectively, leading to $n_L = \Gamma_e/r_0$, where Γ_e is the EIT.

The normal stress n_E inducing the deformation and arising from the external forcing on the drop deserves a further discussion. When investigating the limits of the SDT technique, as early as in 1982, Currie and Van Nieuwkoop observed that in any spinning capillary the background fluid is not at rest, but rather flows towards the axis of the capillary at the center of the drop, thus inducing an extra normal stress on the drop surface [25,33]. This secondary recirculating flow pushing on the drop surface originates from the jump in centripetal pressure at the drop head, between regions I and II in Fig. 5. The origin of this jump is easily understood by recalling that the hydrostatic pressure induced by the rotational acceleration is proportional to the fluid density, which is smaller in the drop as compared to the background fluid. By numerically solving the Navier-Stokes equations [34], we verified that this secondary flow gives rise to a velocity field with a radial component directly proportional to ΔP_ω [32]. Since the external forcing on the drop originates from the secondary recirculating flow and the latter is proportional to ΔP_ω, we write $n_E = \alpha \Delta P_\omega$ with α a positive constant.

Equation (6) can then be rewritten as

$$\alpha \Delta P_\omega - \frac{2\eta_e v}{l} - \frac{\Gamma_e}{r_0} = 0, \tag{7}$$

which yields for the radial deformation velocity

$$v = \frac{\alpha l}{2\eta_e}\Delta P_\omega - \frac{\Gamma_e l}{2 r_0 \eta_e}, \tag{8}$$

i.e., the linear form introduced empirically in Eq. (5). Note that for miscible fluids Γ_e decreases over time, such that Eq. (8) holds only for short times after the onset of the radial deformation, well before diffusion smears out the interface. For this reason, we measure the dynamics of the drop deformation only for a few seconds, before diffusion becomes significant.

Albeit simple, Eq. (8) allows all the main features of the experimental data of Fig. 4(b) to be rationalized: the velocity of the radial deformation at the onset of the instability varies linearly with the centripetal forcing ΔP_ω, with a prefactor that does not depend on the specific parameters of the drop fluid, namely its viscosity and water concentration c_w. Furthermore, Eq. (8) contains an offset proportional to Γ_e, which for miscible fluids is expected to depend on the concentration gradient according to Eq. (1), and thus to be more significant at the highest c_w. This explains why the data for $c_w \geqslant 0.9$ in Fig. 4(b) are not compatible with a line passing through the origin. Figure 6(a) shows a master curve obtained by fitting each dataset at a given water concentration with Eq. (8) and then rescaling the data using the parameters resulting from the best fit, by defining the scaled variables $v' = (v\frac{r_0}{l} + \frac{\Gamma_e}{2\eta_e})\frac{2\eta_e}{\alpha}$ and $P' = r_0 \Delta P_\omega$. In this representation, the data should fall on the straight line $v' = P'$. Figure 6 shows that within experimental error this is indeed the case, and that the results do not depend on the fluorescein concentration.

The values of Γ_e used to rescale the data in Fig. 6(a) are shown in Fig. 6(b) as a function of the volume fraction ϕ and mass fraction c_w of water in the drop, where solid and open symbols refer to two concentrations of fluorescein. It is worth emphasizing the ultralow value of the EIT, which attains at most 250 ± 50 nN/m for pure water drops in pure glycerol. This value is much lower

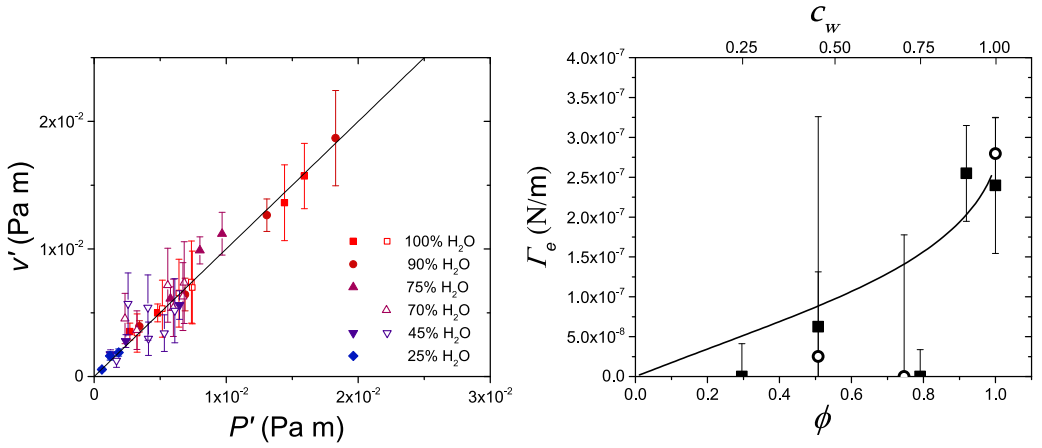

FIG. 6. (a) Mastercurve of the data of Fig. 4(b), obtained by using the scale variable introduced in the text. (b) Experimental values of Γ_e used to rescale the data in panel (a) as a function of the water volume fraction ϕ (bottom axis) and the correspondent water mass fraction c_w (top axis) in the drop. The black line is the theoretical prediction for Γ_e [Eq. (10)], discussed in the text. In both panels, solid (open) points refer to measurements with fluorescein concentration 2×10^{-3} wt/wt (10^{-3} wt/wt).

than that previously reported in literature [23]. Our findings solve the longstanding controversy stemming from conflicting literature values for the same system [23,24,35], as mentioned in Sec. I. In particular, our result is in stark contrast with the value of EIT between water and glycerol reported in [23], $\Gamma_e = 0.58$ mN/m. Note that this latter value is also in contrast with the experimental observation that drops of pure water spinning in glycerol keep on elongating without reaching a stationary state, even in experiments lasting thousands of seconds. If the EIT was as high as reported in [23], a drop of water in glycerol would deform towards a stationary state following an exponential relaxation with time constant $\tau \simeq 1.4$ s, estimated following Ref. [16] and assuming a relaxation dynamics similar to that of drops spinning in an immiscible background fluid. This is clearly not the case. By contrast, the ultralow magnitude of the EIT measured here (a few hundreds of nN/m) is consistent with several works [24,36,37] that report a negligible EIT for the same system.

A further support to our findings comes from a review of previous works investigating the Saffman-Taylor instability occurring when water is injected in a Hele-Show cell containing glycerol. Although a Saffman-Taylor instability does occur a few ms after the injection of the less viscous fluid (water) into a Hele-Shaw cell and hence reduces the effects of diffusion, its visualization has systematically suggested that viscous dissipation largely dominates over interfacial effects. In this limit, the wavelength of the instability λ_{ST} is only dictated by the gap of the injection cell b, and is expected to satisfy

$$4b \lesssim \lambda_{ST} \lesssim 5b. \tag{9}$$

Previous works by Paterson [35] and more recently by Bischofberger and coworkers [36] and Lajeunesse and coworkers [37] systematically find λ_{ST} values in this regime, thus suggesting that the EIT between water and glycerol is too low to be measurable through the Saffman-Taylor instability. To corroborate this notion, we use Eq. (9) to extract a lower bound for the Γ_e values measurable with this technique [38,39], which we quantify as the EIT for which the wavelength observed at the onset of the instability equals $4b$. We show in [32] that this lower bound for water-glycerol systems in a typical Hele-Show cell and for accessible injection rates is approximately 0.1 mN/m, while the measurement of much lower values is hampered by diffusion.

By contrast, the analysis of the radial deformation of drops towards dumbbell shapes proposed here allows one to measure EIT values as low as hundreds of nN/m, well beyond the limits of any other standard experimental technique. The strength of the method proposed in this work resides in the fact that the forcing $\alpha \Delta P_\omega$ is very weak, thus allowing relatively low values of the capillary (Ca) and the Bond (Bo) numbers to be reached. The first is defined as the ratio between viscous forces and surface tension forces acting across the interface between the fluids: $\mathrm{Ca} = \frac{\eta v}{\Gamma}$. Considering the viscosity of the background fluid (glycerol), the measured deformation speed v and Γ_e, the capillary numbers characterizing our experiments are in the range $2 \lesssim \mathrm{Ca} \lesssim 20$, which are relatively low, taking into account that we probe miscible interfaces and hence Γ_e is very small. The second dimensionless number relevant for our experiments is the Bond number, the ratio of the external forces to surface tension forces: $\mathrm{Bo} = \alpha \Delta P_\omega r_0 / \Gamma_e$. In our case, $0.4 \lesssim \mathrm{Bo} \lesssim 4$, corroborating a scenario where capillary stresses are indeed relevant for the drop deformation. The estimates for Ca and Bo also explain the large uncertainty on the value of Γ_e at $\varphi < 0.9$ in Fig. 6(b): when the EIT decreases to extremely low values, both the capillary and the Bond number increase well above unity, making Γ_e barely measurable.

In order to further validate our measurements, we calculate the expected EIT between water and glycerol using a phase field model introduced in [5]. We briefly recall the main ingredients of the model: by assuming local equilibrium between the two fluids [40–42], one computes both the enthalpic and the entropic contributions to the Korteweg parameter $\kappa(\tilde{\varphi})$ using lattice theory arguments and assuming for simplicity that the mixture is symmetric, i.e., that the two fluids have the same molecular volume. The two terms are due, respectively, to the variation of the internal energy density u and to the decrease of configurational entropy density s in the region where $|\nabla \tilde{\varphi}| > 0$. They are obtained by expressing u and s as a function of the local concentration, assuming a concentration gradient across three adjacent lattice layers orthogonal to the z direction, and finally by expanding the local concentration around that of the central layer, up to second order in the spatial derivatives of $\tilde{\varphi}$. Furthermore, in analogy to equilibrium systems, the local concentration profile is modeled by $\tilde{\varphi} = \frac{\phi}{2} + \frac{\phi}{2} \tanh(\frac{z}{\delta})$, with ϕ the volume fraction of one kind of molecules, e.g., water, in the bulk fluids. As detailed in Ref. [5], the model predicts

$$\Gamma_e = \frac{RTa^2}{V_m \delta} \left\{ \chi_{wg} \frac{\phi^2}{6} + \frac{2}{3} \left[1 + \frac{1-\phi}{\phi} \ln(1-\phi) \right] \right\}, \tag{10}$$

with R the ideal gas constant, a and V_m the diameter and the molar volume of the fluid molecules respectively, and δ the interface thickness. The first term on the right-hand side of Eq. (10), proportional to the χ_{wg} parameter characterizing the interaction between water and glycerol molecules, quantifies the energy penalty (or gain) due to a local compositional inhomogeneity. The second term is always positive and depends only on ϕ. It quantifies the entropy loss due to the (transient) gradient of concentration. We note that the approximations used to derive Eq. (10) imply that the concentration gradient at the interface is small, such that the effective interfacial tension is dominated by the first term of the mixing free energy expansion, i.e., the square gradient one.

To estimate Γ_e for our water-glycerol mixtures we use Eq. (10) and take the average of the molecular diameter and molar volume of water and glycerol: $\langle a \rangle = 0.45$ nm and $\langle V_m \rangle = 45.5$ ml/mol. We further consider the effect of diffusion by calculating the thickness of the interface as $\delta = \sqrt{2 D_{wg} t}$ where $D_{wg} = 1.4 \times 10^{-11}$ m^2/s is the diffusion coefficient of water in glycerol [27] and $t \approx 15$ s is the typical time elapsing between the drop injection and the observation of the instability. The result is displayed in Fig. 6(b) (line), showing that our data are very well captured by the theoretical Γ_e obtained via Eq. (10), with no adjustable parameter. The agreement between the data and Eq. (10) suggests that the model of Ref. [5], albeit very simple, may be reliably used to estimate the EIT. Since $-1 < \chi < 1$ for most pairs of miscible substances [43], for $\phi \backsimeq 1$ the effective interfacial tension between miscible molecular fluids is well approximated by

$$\Gamma_e \approx \frac{2RTa^2}{3V_m \delta}. \tag{11}$$

As an example, for liquids with characteristics similar to water ($a \approx 0.1$ nm, $V_m = 18$ ml/mol, $D = 1.025 \times 10^{-9}$ m^2/s [27] at $T = 298.15$ K), Eq. (11) predicts a tension ranging from $\Gamma_e \approx 13$ mN/m to $\Gamma_e \approx 20 \times 10^{-6}$ mN/m as the interface thickness increases from a value comparable to the molecular size ($\delta \approx a$ for $t = 0$) to 45 μm after $t = 1$ s of interdiffusion. This supports the fact that for fully miscible low-viscosity fluids capillary effects decay very rapidly with time and can be safely neglected in most cases. However, this may not be the case when diffusivity is very low, a condition that can be attained in many simple liquids like silicon oils [44], colloidal and polymer suspensions [5], or in geologically relevant fluids such as silicate fluids in the Earth mantle [45,46]. Finally, we note that this argument offers also a possible explanation for the absence of deformation for the triethylene glycol drop in Fig. 1, panel B. Indeed, TEG has a miscibility with glycerol similar to that of water, the three liquids having similar Hansen solubility parameters [47], but it is significantly more viscous than water ($\eta_{\mathrm{TEG}} = 49$ mPa s). Therefore, one may expect, on the timescale of our experiments, a stronger effect of the EIT as compared to the case of water drops, thus preventing the development of the dumbbell shape.

IV. CONCLUSIONS

We have experimentally characterized the time evolution of the shape of miscible drops in SDT experiments. We have shown that a dumbbell shape arises for sufficiently low values of EIT, which depends not only on the density and viscosity contrast between the drop and the background fluids, but also on the molecular structure of the fluids. We have focused on mixtures of water and glycerol, for which literature data were conflicting [23,24,35], and employed the dynamics of the drop shape as a tool to measure the EIT. By means of a simple model which takes into account the normal stress on the drop surface, the shear stress opposing the deformation, and a Laplace-like term containing an effective interfacial tension, we obtained an EIT of 250 ± 50 nN/m for water in contact with pure glycerol, decreasing rapidly below the resolution limit of the method as the amount of glycerol in the drops increases above 10%. This result is in excellent agreement with an estimate of the order of magnitude for the EIT for the same system obtained from a phase field model [5], while it is orders of magnitude lower than the experimental limit of all conventional techniques for measuring interfacial tensions. Therefore, besides shedding light on the controversy stemming from conflicting literature data on the EIT between water and glycerol, our work demonstrates a new method to measure extremely low interfacial tensions and in particular the EIT, paving the way for a thorough understanding of Korteweg stresses and capillary phenomena in miscible fluids.

ACKNOWLEDGMENTS

We gratefully acknowledge support from the Centre National d'Études Spatiales (CNES). We thank Lucio Isa for fruitful discussions.

[1] J. S. Rowlinson and B. Widom, *Molecular Theory of Capillarity* (Dover, Mineola, NY, 2002).

[2] D. J. Korteweg, Sur la forme qui prennent les équations du movement des fluides si l'on tient compte des forces capillaires causées par des variations de densité considérable mais continues et sur la théorie de la capillarité dans l'hypothèse d'une variations continue de la densité, Arch. Neerl. Sci. Exactes Nat. **6**, 1 (1901).

[3] J. W. Cahn and J. E. Hilliard, Free energy of a nonuniform system. I. Interfacial free energy, J. Chem. Phys. **28**, 11 (1958).

[4] D. Truzzolillo and L. Cipelletti, Off-equilibrium surface tension in miscible fluids, Soft Matter **13**, 13 (2017).

[5] D. Truzzolillo, S. Mora, C. Dupas, and L. Cipelletti, Nonequilibrium Interfacial Tension in Simple and Complex Fluids, Phys. Rev. X **6**, 041057 (2016).

[6] P. Cicuta, A. Vailati, and M. Giglio, Capillary-to-bulk crossover of nonequilibrium fluctuations in the free diffusion of a near-critical binary liquid mixture, Appl. Opt. **40**, 4140 (2001).
[7] A. Vorobev, T. Zagvozkin, and T. Lyubimova, Shapes of a rising miscible droplet, Phys. Fluids **32**, 012112 (2020).
[8] L. K. Antanovskii, Microscale theory of surface tension, Phys. Rev. E **54**, 6285 (1996).
[9] M. Bier, Nonequilibrium interfacial tension during relaxation, Phys. Rev. E **92**, 042128 (2015).
[10] A. Vorobev and A. Boghi, Phase-field modelling of a miscible system in spinning droplet tensiometer, J. Colloid Interface Sci. **482**, 193 (2016).
[11] C.-Y. Chen and E. Meiburg, Miscible displacements in capillary tubes. Part 2. Numerical simulations, J. Fluid Mech. **326**, 57 (1996).
[12] C.-Y. Chen and E. Meiburg, Miscible displacements in capillary tubes: Influence of Korteweg stresses and divergence effects, Phys. Fluids **14**, 2052 (2002).
[13] V. Shevtsova, Y. A. Gaponenko, V. Yasnou, A. Mialdun, and A. Nepomnyashchy, Two-scale wave patterns on a periodically excited miscible liquid-liquid interface, J. Fluid Mech. **795**, 409 (2016).
[14] S. E. May and J. V. Maher, Capillary-Wave Relaxation for A Meniscus between Miscible Liquids, Phys. Rev. Lett. **67**, 2013 (1991).
[15] J. A. Pojman, C. Whitmore, M. L. Turco Liveri, R. Lombardo, J. Marszalek, R. Parker, and B. Zoltowski, Evidence for the existence of an effective interfacial tension between miscible fluids: Isobutyric acid-water and 1-butanol-water in a spinning-drop tensiometer, Langmuir **22**, 2569 (2006).
[16] A. Carbonaro, L. Cipelletti, and D. Truzzolillo, Spinning drop dynamics in miscible and immiscible environments, Langmuir **35**, 11330 (2019).
[17] K. Gowda. V, C. Brouzet, T. Lefranc, L. D. Söderberg, and F. Lundell, Effective interfacial tension in flow-focusing of colloidal dispersions: 3-D numerical simulations and experiments, J. Fluid Mech. **876**, 1052 (2019).
[18] S. Bamberger, G. V. Seaman, K. Sharp, and D. E. Brooks, The effects of salts on the interfacial tension of aqueous dextran poly(ethylene glycol) phase systems, J. Colloid Interface Sci. **99**, 194 (1984).
[19] Y. Liu, R. Lipowsky, and R. Dimova, Concentration dependence of the interfacial tension for aqueous two-phase polymer solutions of dextran and polyethylene glycol, Langmuir **28**, 3831 (2012).
[20] B. Vonnegut, Rotating bubble method for the determination of surface and interfacial tensions, Rev. Sci. Instrum. **13**, 6 (1942).
[21] G. Viner, T. La Monica, R. Lombardo, and J. A. Pojman, Effect of pseudo-gravitational acceleration on the dissolution rate of miscible drops, Chaos **27**, 104603 (2017).
[22] B. Zoltowski, Y. Chekanov, J. Masere, J. A. Pojman, and V. Volpert, Evidence for the existence of an effective interfacial tension between miscible fluids. 2. Dodecyl acrylate-poly(dodecyl acrylate) in a spinning drop tensiometer, Langmuir **23**, 5522 (2007).
[23] P. Petitjeans, Une tension de surface pour le fluides miscibles, C.R. Acad Sci. Paris **322**, 673 (1996).
[24] M. Legendre, P. Petitjeans, and P. Kurowski, Instabilités à l'interface entre fluides miscibles par forçage oscillant horizontal, C.R. Mec. **331**, 617 (2003).
[25] C. D. Manning and L. E. Scriven, On interfacial tension measurement with a spinning drop in gyrostatic equilibrium, Rev. Sci. Instrum. **48**, 1699 (1977).
[26] *Physical Properties of Glycerine and its Solutions* (Glycerine Producers' Association, New York, 1963).
[27] G. D'Errico, O. Ortona, F. Capuano, and V. Vitagliano, Diffusion coefficients for the binary system glycerol + water at 25 °C. A velocity correlation study, J. Chem. Eng. Data **49**, 1665 (2004).
[28] P. Galambos and F. K. Forster, in *Micro Total Analysis Systems 98*, edited by D. J. Harrison and A. van den Berg (Springer, Netherlands, Dordrecht, 1998), pp. 189–192.
[29] J. R. Lister and H. A. Stone, Time-dependent viscous deformation of a drop in a rapidly rotating denser fluid, J. Fluid Mech. **317**, 275 (1996).
[30] M. R. Spiegel and L. J. Stephens, *Statistics* (McGraw-Hill, New York, 2008).
[31] W. H. Press, S. A. Teukolsky, W. T. Vetterling, and B. P. Flannery, *Numerical Recipes in Fortran: The Art of Scientific Computing* (Cambridge University Press, Cambridge, 1996).
[32] See Supplemental Material at http://link.aps.org/supplemental/10.1103/PhysRevFluids.5.074001 for (i) the statistical significance of the c_w dependence of the deformation velocity, (ii) simulations of the

recirculating flow on top of spinning drops and the dependence of the flow on ΔP_ω, and (iii) the limitations of the direct visualization of the radial Saffman-Taylor instability as a method to measure the effective interfacial tension in water-glycerol systems.

[33] P. Currie and J. Van Nieuwkoop, Buoyancy effects in the spinning-drop interfacial tensiometer, J. Colloid Interface Sci. **87**, 301 (1982).

[34] A. Quarteroni, *Numerical Models for Differential Problems*, Modeling, Simulation and Applications, Vol. 16 (Springer International, Cham, 2017).

[35] L. Paterson, Fingering with miscible fluids in a Hele Shaw cell, Phys. Fluids **28**, 26 (1985).

[36] I. Bischofberger, R. Ramachandran, and S. R. Nagel, Fingering versus stability in the limit of zero interfacial tension, Nat. Commun. **5**, 5265 (2014).

[37] E. Lajeunesse, J. Martin, N. Rakotomalala, and D. Salin, 3D Instability of Miscible Displacements in A Hele-Shaw Cell, Phys. Rev. Lett. **79**, 5254 (1997).

[38] J. Miranda and M. Widom, Radial fingering in a Hele-Shaw cell: A weakly nonlinear analysis, Physica D **120**, 315 (1998).

[39] D. Truzzolillo, S. Mora, C. Dupas, and L. Cipelletti, Off-Equilibrium Surface Tension in Colloidal Suspensions, Phys. Rev. Lett. **112**, 128303 (2014).

[40] L. Jinwoo and H. Tanaka, Local non-equilibrium thermodynamics, Sci. Rep. **5**, 7832 (2015).

[41] D. Truzzolillo and L. Cipelletti, Hydrodynamic instabilities in miscible fluids, J. Phys.: Condens. Matter **30**, 033001 (2018).

[42] A. Kheniene and A. Vorobev, Linear stability analysis of a horizontal phase boundary separating two miscible liquids, Phys. Rev. E **88**, 022404 (2013).

[43] A. F. M. Barton, *Handbook of Poylmer-Liquid Interaction Parameters and Solubility Parameters* (CRC, Boca Raton, FL 1990).

[44] J. Kuang, T. Maxworthy, and P. Petitjeans, Miscible displacements between silicone oils in capillary tubes, Eur. J. Mech. B **22**, 271 (2003).

[45] G. Morra and D. A. Yuen, Role of Korteweg stresses in geodynamics, Geophys. Res. Lett. **35**, L07304 (2008)

[46] J. E. Mungall, Interfacial Tension in Miscible Two-Fluid Systems with Linear Viscoelastic Rheology, Phys. Rev. Lett. **73**, 288 (1994).

[47] C. M. Hansen, *Hansen Solubility Parameters - A User's Handbook* (CRC, Boca Raton, FL, 2000).